

Flexible FTN-OTFS for High-Mobility LEO Satellite-to-Ground Communication

Chaorong Zhang, Hui Xu, Benjamin K. Ng, Yue Liu, Chan-Tong Lam, and Halim Yanikomeroglu

Abstract—In this paper, a lightweight LEO satellite-assisted flexible faster-than-Nyquist (FTN)-orthogonal time frequency space (OTFS) (LEO-FFTN-OTFS) scheme is proposed to address the stringent constraints on onboard power consumption and the severe impact of fast time-varying channels in non-terrestrial networks. A rigorous system framework incorporating realistic 3GPP Tapped Delay Line (TDL) channel models is established to accurately capture high-mobility propagation characteristics. To counteract channel aging effects while maintaining low computational complexity, an SNR-aware flexible FTN strategy is introduced, wherein a low-complexity Look-Up Table (LUT) is utilized to adaptively optimize the time-domain compression factor based on instantaneous channel responses. Through this mechanism, the trade-off between rate acceleration and interference penalty is effectively resolved, ensuring that spectral efficiency is maximized while strict reliability constraints are satisfied with minimal processing overhead. Moreover, a comprehensive theoretical analysis is provided, in which analytical expressions for effective throughput, energy efficiency, and bit error rate are derived. Finally, it is demonstrated by extensive simulations that the proposed scheme significantly outperforms static FTN benchmarks, offering a superior balance of high throughput and robustness for next-generation LEO communications.

Index Terms—LEO satellite, OTFS, Faster-than-Nyquist

I. INTRODUCTION

A. Low Earth Orbit Satellite

The integration of non-terrestrial networks (NTN) into the envisioned 6G ecosystem has positioned *Low Earth Orbit* (LEO) satellite communications as a pivotal technology for achieving ubiquitous, three-dimensional global connectivity [1]. Unlike their geostationary (GEO) and medium earth orbit (MEO) counterparts, LEO constellations operate at significantly lower altitudes, typically at altitudes of 500-2000 km, offering intrinsic advantages such as negligible propagation latency and reduced path loss [2]. These characteristics make LEO satellites indispensable for supporting delay-sensitive applications, ranging from autonomous driving and remote industrial control to emergency disaster relief. However, these benefits come at the cost of extreme satellite mobility [3]. The relative velocity between LEO satellites and ground user equipment (UE) can exceed 7.6 km/s, inducing severe Doppler shifts and rapid channel time-variations. Such harsh conditions disrupt the orthogonality of subcarriers in conventional Orthogonal Frequency Division Multiplexing (OFDM), leading

(Corresponding author: Benjamin K. Ng.) Chaorong Zhang, Hui Xu, Benjamin K. Ng, Yue Liu and Chan-Tong Lam are with the Faculty of Applied Sciences, Macao Polytechnic University, Macao SAR, China. Halim Yanikomeroglu is with System and Computer Engineering Department, Carleton University, Ottawa, ON K1S 5B6, Canada.

to catastrophic inter-carrier interference (ICI) and significantly degrading link performance.

B. Orthogonal Time Frequency Space

To navigate this high-mobility landscape, *orthogonal time frequency space* (OTFS) modulation has emerged as a revolutionary waveform paradigm [4]. By transforming the information symbols into the Delay-Doppler (DD) domain rather than the traditional Time-Frequency (TF) domain, OTFS converts the rapidly fading, doubly-selective channel into a quasi-static, sparse interaction [5]. This domain transformation allows the receiver to separate multipath delays and Doppler shifts, effectively converting multiplicative fading into a simpler convolutional interaction. Compared to other newly proposed waveforms such as Affine Frequency Division Multiplexing (AFDM) or Orthogonal Delay-Doppler Modulation (ODDM) [6], OTFS offers a distinct advantage: it fully exploits the diversity across the entire time-frequency grid through 2D spreading. This mechanism provides enhanced resilience against fractional Doppler shifts and eliminates the need for complex chirp parameter tuning, making it a robust candidate for the unpredictable LEO environment.

C. Faster-than-Nyquist

Despite its unparalleled robustness against mobility, standard OTFS is theoretically bounded by the Nyquist limit, which imposes a fundamental restriction on spectral efficiency (SE). This limitation is particularly critical in satellite communications, where spectrum resources are exceedingly scarce and expensive. While SE can theoretically be improved by adopting higher-order modulation schemes, e.g., 64-QAM or 256-QAM, this approach incurs a prohibitive penalty in terms of the required signal-to-noise ratio (SNR). Furthermore, higher-order modulations result in a high Peak-to-Average Power Ratio (PAPR), rendering the signal sensitive to the nonlinearities of satellite on-board High-Power Amplifiers (HPAs) [7]. To break this bottleneck without overburdening the power budget, *Faster-than-Nyquist* (FTN) signaling offers a more power-efficient alternative [8]. By intentionally compressing pulse intervals in the time domain beyond the orthogonal limit, FTN packs more data into the same bandwidth, thereby approaching channel capacity limits at the expense of introducing controlled inter-symbol interference (ISI) [9].

However, the direct application of conventional, fixed-parameter FTN strategies to LEO links proves to be suboptimal due to the highly dynamic nature of the satellite pass. As an LEO satellite traverses its orbit from the horizon to

the zenith and back to the horizon, the link geometry and channel conditions fluctuate drastically [10]. At low elevation angles, the link suffers from severe path loss, atmospheric attenuation, and shadowing, resulting in a low SNR regime. In this scenario, a static, aggressive FTN compression factor would exacerbate ISI beyond the decoder's capability, causing link outages. Conversely, at high elevation angles, the channel effectively becomes a Line-of-Sight (LOS) link with high SNR. Here, a conservative compression factor fails to fully exploit the superior channel conditions, leading to a waste of valuable spectral resources. Consequently, a “one-size-fits-all” FTN approach is ill-suited for NTN. To fully unleash the potential of next-generation satellite networks, a flexible FTN (FFTN) strategy that is adaptively tailored to the time-varying LEO environment is essential.

D. Related Works and Contributions

LEO satellite-assisted OTFS systems [11], [12] generally suffer from limited SE due to the inherent Nyquist constraint. Although high-order modulation or other complex schemes may be conventional approaches to enhance SE, it is impractical here due to the prohibitive cost of replenishing the limited onboard energy of LEO satellites. Furthermore, given the inherent high complexity of OTFS, a lightweight design is strictly required to offset the processing overhead while effectively resisting fast time-varying channel effects. While the integration of FTN [13], [14] offers a potential remedy by improving SE without increasing the constellation size, existing works are predominantly restricted to terrestrial networks with normalized channel assumptions. Crucially, they rely on suboptimal fixed compression factors, which fail to accommodate the drastic link quality fluctuations characteristic of LEO satellite passes. Specifically, the LEO downlink exhibits a distinct “horizon-to-zenith” evolution pattern. In such a highly dynamic environment, a static FTN strategy faces a fundamental dilemma: a conservative compression factor incurs a significant opportunity cost in spectral efficiency during the benign zenith phase, whereas an aggressive factor leads to irreducible error floors and potential link outages during the signal-impaired horizon phase. Consequently, a paradigm shift from static parameter configuration to channel-aware adaptability is imperative to resolve this conflict. To fully exploit the dynamic LEO channel capacity with minimal computational complexity, we propose a promising lightweight LEO satellite-assisted Flexible FTN-OTFS (LEO-FFTN-OTFS) scheme.

Overall, the main contributions of this work are summarized as follows:

- **Rigorous System Framework for LEO Channels:**

We pioneer the investigation of FTN-OTFS in high-mobility LEO satellite environments by establishing a rigorous system framework. Unlike generic models, our approach incorporates various realistic 3GPP Tapped Delay Line (TDL) channel profiles that explicitly account for elevation-dependent propagation characteristics, ranging from Non-Line-of-Sight (NLoS) scattering at low elevation angles to LoS dominance at the zenith.

- **SNR-Aware Flexible FTN Strategy:** We propose a tailored FFTN transmission strategy that adopts a

lightweight design philosophy to handle the rapid time-variation of LEO links. By utilizing a low-complexity Look-Up Table (LUT) to ensure real-time adaptability, this mechanism allows the system to opportunistically exploit high-SNR windows for rate acceleration while reverting to robust modes during deep fades, effectively resolving the trade-off between spectral efficiency and link outage risks.

- **Comprehensive Analysis and Validation:** We provide a comprehensive theoretical analysis, deriving analytical expressions for throughput, energy efficiency (EE), and bit error rate (BER) bounds. Simulation and theoretical results offer some insights into the trade-offs between SE and reliability in LEO wireless networks.

E. Organization

The remainder of this paper is organized as follows. Section II presents the system model of the LEO satellite-assisted FTN-OTFS transmission and characterizes the high-mobility LEO channel using 3GPP TDL profiles. Section III details the proposed SNR-aware FFTN strategy, including the problem formulation and the low-complexity LUT-based adaptation protocol. Section IV presents a comprehensive performance analysis, deriving analytical expressions for effective throughput, SE, EE, and theoretical BER bounds. Numerical results and discussions are provided in Section V, followed by conclusions in Section VI.

F. Notation

Throughout this paper, scalars are denoted by italic letters, e.g., a , vectors by boldface lower-case letters (e.g., \mathbf{a}), and matrices by boldface upper-case letters, e.g., \mathbf{A} . The superscripts $(\cdot)^T$ and $(\cdot)^H$ represent the transpose and the Hermitian (conjugate) transpose operations, respectively. $\mathbb{C}^{M \times N}$ denotes the set of $M \times N$ complex-valued matrices. $\mathbb{E}[\cdot]$ denotes the statistical expectation operator, and $|\cdot|$ represents the absolute value of a scalar or the cardinality of a set. $\|\cdot\|$ denotes the Euclidean norm of a vector. The symbol \otimes stands for the Kronecker product, and $\mathcal{CN}(\mu, \sigma^2)$ represents the circularly symmetric complex Gaussian distribution with mean μ and variance σ^2 .

II. SYSTEM MODEL

A. Transmitter Design and FTN Signaling

In this work, we first investigate a downlink LEO satellite communication single-input single-output (SISO) system employing standard FTN-aided OTFS modulation. The DD plane is discretized into a grid of size $M \times N$, where M and N denote the number of delay and Doppler bins, respectively. Let $\mathbf{X}^{\text{DD}} \in \mathbb{C}^{M \times N}$ represent the transmitted symbol matrix, where the entry $x[l, k]$ corresponds to the M_{mod} -ary QAM symbol at the l -th delay and k -th Doppler index.

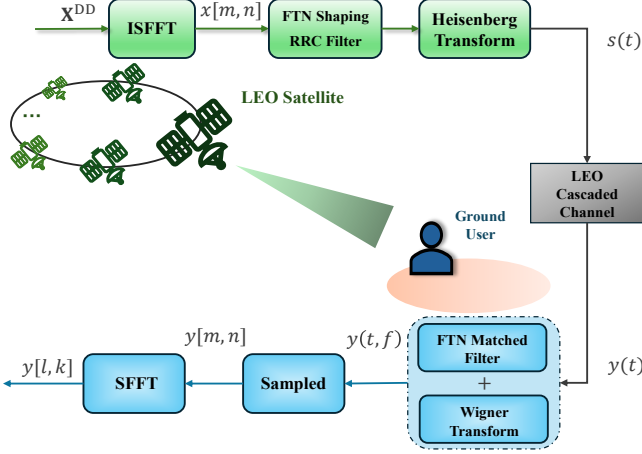


Fig. 1. System model and signal processing.

The modulation process begins with the Inverse Symplectic Fast Fourier Transform (ISFFT), mapping the DD domain symbols to the Time-Frequency (TF) domain as

$$X[m, n] = \frac{1}{\sqrt{MN}} \sum_{l=0}^{M-1} \sum_{k=0}^{N-1} x[l, k] e^{j2\pi \left(\frac{ml}{M} - \frac{nk}{N} \right)}, \quad (1)$$

where $m \in [0, M - 1]$ and $n \in [0, N - 1]$.

To enhance SE, we introduce time-domain FTN signaling characterized by a compression factor $\alpha \in (0, 1]$. The FTN-specific symbol duration is defined as $T_F = \alpha T_0$, where $T_0 = 1/M$ represents the Nyquist symbol interval and T is the frame duration. Consequently, the subcarrier spacing remains fixed at $\Delta f = 1/T$. Subsequently, the Heisenberg transform, combined with an FTN pulse shaping filter $g_{tx}(t)$, generates the continuous time-domain signal $s(t)$:

$$s(t) = \sum_{m=0}^{M-1} \sum_{n=0}^{N-1} X[m, n] g_{tx}(t - nT_F) e^{j2\pi m \Delta f (t - nT_F)}, \quad (2)$$

where $g_{tx}(t)$ is typically a Root Raised Cosine (RRC) pulse. The impact of the compression factor α is visually demonstrated in Fig. 2. In Fig. 2 (a), the adoption of $\alpha = 0.8$ forces the pulses closer together, causing non-zero distinct values of adjacent pulses to overlap at the sampling instant. This phenomenon intentionally introduces ISI to boost the transmission rate. Furthermore, also as shown in Fig. 2 (b), this non-orthogonal transmission results in a spectral dip compared to the flat spectrum of Nyquist signaling, effectively acting as a frequency-selective channel or introducing colored noise.

B. LEO Wireless Environments

The forward link channel between the LEO satellite and the ground user equipment (UE) is characterized by a combination of large-scale path loss and small-scale multipath fading. Unlike terrestrial models that often assume static channel gains, our model explicitly accounts for the dynamic link geometry and Doppler shifts unique to LEO constellations.

1) *Large-Scale Path Loss Modeling*: The forward link budget is primarily governed by the large-scale path loss L (in dB), which aggregates geometric spreading, terrestrial

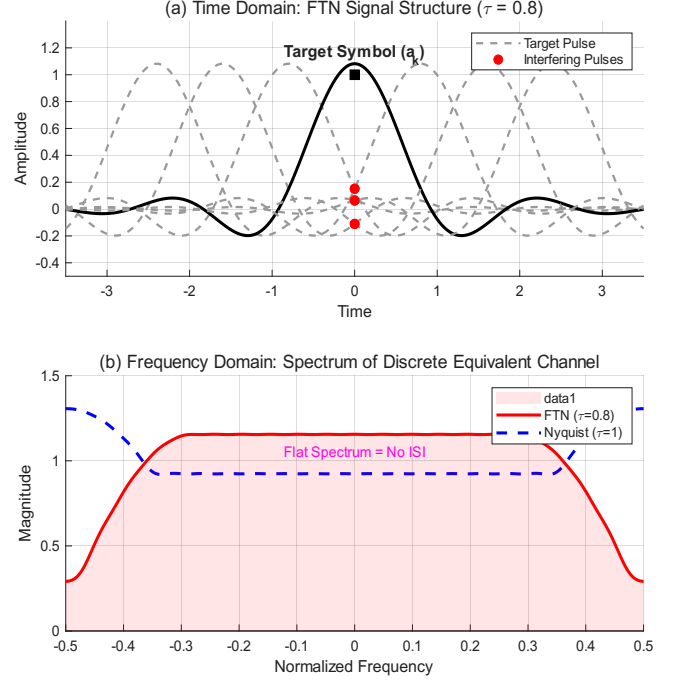


Fig. 2. FTN showcase.

blockage, and atmospheric impairments. Aligning with the ITU-R P.618 guidelines for NTN [15], [16], the total path loss is expressed as:

$$L = L_b + L_g + L_s, \quad (3)$$

where L_b , L_g , and L_s denote the basic path loss, atmospheric gas attenuation, and scintillation loss, respectively.

The basic path loss L_b accounts for the deterministic free-space propagation and stochastic environmental shadowing. It is composed of the Free-Space Path Loss (FSPL), Shadow Fading (SF), and Clutter Loss (CL):

$$L_b = \text{FSPL}(d, f_c) + \text{SF} + \text{CL}(\theta_E, f_c). \quad (4)$$

Here, $\text{SF} \sim \mathcal{N}(0, \sigma_{\text{SF}}^2)$ represents log-normal shadow fading caused by local obstacles. The FSPL is determined by the carrier frequency f_c (in GHz) and the instantaneous slant distance d (in meters) as follows:

$$\text{FSPL}(d, f_c) = 32.45 + 20 \log_{10}(f_c) + 20 \log_{10}(d). \quad (5)$$

Given the highly dynamic nature of LEO constellations, the slant distance d varies significantly with the time-dependent elevation angle θ_E . Based on the Earth-centered geometric model with Earth radius $R_E \approx 6371$ km and satellite altitude h_0 , d is derived as:

$$d = \sqrt{R_E^2 \sin^2(\theta_E) + h_0^2 + 2h_0 R_E - R_E \sin(\theta_E)}. \quad (6)$$

To accurately capture terrestrial propagation characteristics, particularly in urban canyons where buildings obstruct signals, we model the Clutter Loss (CL) as a function of both frequency and elevation angle:

$$\text{CL}(\theta_E, f_c) = A_{cl} + B_{cl} \log_{10}(f_c) + C (1 - \sin(\theta_E)), \quad (7)$$

where A_{cl} and B_{cl} are frequency-dependent coefficients, and $C = 20$ is an empirical factor for typical urban scenarios. The term $(1 - \sin(\theta_E))$ explicitly models the elevation dependence, reflecting that signals arriving from the zenith (high θ_E) experience minimal clutter attenuation compared to those grazing the horizon.

Furthermore, the signal traverses atmospheric layers, incurring frequency-dependent absorption. According to [17], the atmospheric gas attenuation L_g is modeled as:

$$L_g = \frac{A_{zenith}(f_c)}{\sin(\theta_E)}, \quad (8)$$

where A_{zenith} denotes the specific zenith attenuation. The $1/\sin(\theta_E)$ factor accounts for the increased effective atmospheric path length at lower elevation angles. Finally, scintillation loss L_s , induced by rapid fluctuations in the refractive index due to ionospheric ($f_c < 6$ GHz) or tropospheric ($f_c > 6$ GHz) irregularities [15], [16], is incorporated. Note that rain attenuation is omitted in this study under the clear-sky assumption.

2) *Small-Scale DD Domain Fading*: Superimposed on the large-scale path loss is the small-scale multipath fading. To accurately reflect the characteristics of NTN propagation, we adopt the geometry-based stochastic channel models defined in 3GPP TR 38.811 and TR 38.901 [18], [19].¹ Specifically, the Tapped Delay Line (TDL) models are employed to characterize the multipath power delay profile (PDP). Depending on the satellite elevation angle and terrestrial blockage conditions, different TDL profiles are selected. For low elevation angles or dense urban environments where the direct line-of-sight (LOS) is obstructed, the channel follows TDL-A/B/C models characterized by Non-LOS (NLOS) Rayleigh fading. Conversely, for high elevation angles or open rural areas, TDL-D/E models are adopted to represent LOS scenarios governed by Ricean fading. Detailed values of various TDL models are provided in Table I.

The channel impulse response in the DD domain with P dominant taps is given by:

$$h(\tau, \nu) = \sum_{p=0}^{P-1} h_p \delta(\tau - \tau_p) \delta(\nu - \nu_p), \quad (9)$$

where τ_p and ν_p denote the delay and Doppler shift of the p -th path. The complex channel coefficient h_p is modeled as a Ricean random variable given by:

$$h_p = \sqrt{P_p} \left(\sqrt{\frac{K_p}{K_p + 1}} e^{j\varphi} + \sqrt{\frac{1}{K_p + 1}} h_{sc} \right), \quad (10)$$

where P_p is the normalized power of the p -th tap such that $\sum P_p = 1$, K_p is the Ricean K -factor representing the ratio of LOS to NLOS power, φ is the deterministic phase of the LOS component determined by satellite geometry, and $h_{sc} \sim \mathcal{CN}(0, 1)$ represents the scattered diffuse component.

Following the OTFS grid resolutions, the discrete delay and

¹For the sake of presentation clarity and following [19], [20], we compress the original high-dimensional 3GPP TDL model into an equivalent three-tap representation.

Doppler taps are parameterized as

$$\tau_p = \frac{l_p}{M\Delta f}, \quad \nu_p = \frac{r_p + \kappa_p}{NT_F}, \quad (11)$$

where $l_p \in \mathbb{Z}$ and $r_p \in \mathbb{Z}$ are the integer indices. Crucially, $\kappa_p \in [-\frac{1}{2}, \frac{1}{2})$ models the *fractional Doppler* component derived from the user velocity and satellite motion.² By applying the inverse Symplectic Fast Fourier Transform (ISFFT) along the Doppler dimension, the equivalent time-varying impulse response is expressed as

$$h(t, \tau) = \sum_{p=0}^{P-1} h_p e^{j2\pi\nu_p(t-\tau_p)} \delta(\tau - \tau_p). \quad (12)$$

C. Received Signals and OTFS Demodulation

The received continuous-time baseband signal is:

$$y(t) = \sqrt{10^{-L/10}} \sum_{p=0}^{P-1} h_p e^{j2\pi\nu_p(t-\tau_p)} s(t - \tau_p) + w(t), \quad (13)$$

where L is the path loss in dB defined in (3), and $w(t)$ denotes the complex additive white Gaussian noise (AWGN). At the receiver, a matched RRC filter is employed with $g_{rx}(t) = g_{tx}^*(-t)$. The Wigner transform converts $y(t)$ into the TF domain as

$$y(t, f) = \int g_{rx}^*(t' - t) y(t') e^{-j2\pi f(t' - t)} dt'. \quad (14)$$

Sampling at $(t, f) = (nT_F, m\Delta f)$ yields the discrete TF samples:

$$y[m, n] = y(t, f) \Big|_{t=nT_F, f=m\Delta f}. \quad (15)$$

Finally, the symplectic fast Fourier transform (SFFT) provides the DD-domain observations:

$$y[l, k] = \frac{1}{\sqrt{MN}} \sum_{m=0}^{M-1} \sum_{n=0}^{N-1} y[m, n] e^{-j2\pi(\frac{ml}{M} - \frac{nk}{N})}. \quad (16)$$

We further define the DD-domain resolutions as

$$\Delta\tau = \frac{1}{M\Delta f}, \quad \Delta\nu = \frac{1}{NT_F}. \quad (17)$$

For a propagation path with parameters (τ_p, ν_p) , the corresponding discrete integer taps are obtained by

$$\varepsilon_p = \lfloor \tau_p M\Delta f \rfloor, \quad k_p = \lfloor \nu_p NT_F \rfloor. \quad (18)$$

Let $\mathbf{x}^{\text{DD}} \triangleq \text{vec}(\mathbf{X}^{\text{DD}}) \in \mathbb{C}^{MN \times 1}$ and $\mathbf{y} \triangleq \text{vec}(\mathbf{Y}^{\text{DD}}) \in \mathbb{C}^{MN \times 1}$ denote the vectorized DD-domain transmit and receive symbol blocks, respectively. Due to band-limited pulse shaping and FTN acceleration, the effective channel departs from the ideal block-circulant structure of OTFS and becomes a structured block-Toeplitz matrix. Accordingly, the discrete DD-domain input-output relation is expressed as

$$\mathbf{y} = \mathbf{H}_{\text{eff}} \mathbf{x}^{\text{DD}} + \mathbf{z}^{\text{DD}}, \quad (19)$$

²In practical LEO channels, Doppler shifts are continuous and seldom align exactly with discrete Doppler bins. The fractional term κ_p accounts for this mismatch and avoids modeling artifacts due to quantization errors.

TABLE I
SIMULATION PARAMETERS FOR LEO SATELLITE CHANNEL MODELS

Model	Scenario	Small-Scale Fading	Large-Scale Params
TDL-A	Urban, NLOS $\theta_E = 20^\circ$	Delays: [0, 110, 285] ns Power: [0, -4.7, -6.5] dB, $K = -\infty$	$A_{cl} = 15, B_{cl} = 5$ $\sigma_{SF} = 6$ dB
TDL-B	Urban, NLOS $\theta_E = 30^\circ$	Delays: [0, 105, 275] ns Power: [0, -3.8, -5.2] dB, $K = -\infty$	$A_{cl} = 15, B_{cl} = 5$ $\sigma_{SF} = 6$ dB
TDL-C	Rural, NLOS $\theta_E = 30^\circ$	Delays: [0, 260, 830] ns Power: [0, -3.5, -5.8] dB, $K = -\infty$	$A_{cl} = 5, B_{cl} = 2$ $\sigma_{SF} = 6$ dB
TDL-D	Rural, LOS $\theta_E = 60^\circ$	Delays: [0, 290, 895] ns Power: [0, -4.2, -6.1] dB, $K = 13.3$ dB	$A_{cl} = 5, B_{cl} = 2$ $\sigma_{SF} = 2$ dB
TDL-E	Open, LOS $\theta_E = 85^\circ$	Delays: [0, 150, 350] ns Power: [0, -8.0, -12.0] dB, $K = 22.0$ dB	$A_{cl} = 0, B_{cl} = 0$ $\sigma_{SF} = 2$ dB

where $\mathbf{H}_{\text{eff}} \in \mathbb{C}^{MN \times MN}$ denotes the effective channel matrix.

To explicitly characterize \mathbf{H}_{eff} , we adopt a pulse-shaping-aware DD-domain formulation based on the cross-ambiguity function. We further define

$$\mathcal{A}_g(\tau, \nu) \triangleq \int_{-\infty}^{\infty} g_{\text{tx}}(t) g_{\text{rx}}^*(t - \tau) e^{-j2\pi\nu t} dt, \quad (20)$$

which inherently accounts for FTN-induced non-orthogonality through the sampling interval $T_F = \alpha T_0$. Using the DD grid resolutions in (17), the (u, v) -th entry of \mathbf{H}_{eff} is expressed as

$$[\mathbf{H}_{\text{eff}}]_{u,v} = \sqrt{10^{-L/10}} \sum_{p=0}^{P-1} h_p e^{j\varphi_p(u,v)} \times \mathcal{A}_g((l - l')\Delta\tau - \tau_p, (k - k')\Delta\nu - \nu_p). \quad (21)$$

where $u = l + kM$ and $v = l' + k'M$ are the vectorized indices corresponding to DD coordinates (l, k) and (l', k') , respectively. Moreover, $\varphi_p(u, v) = 2\pi\nu_p(t_{\text{eff}} - \tau_p)$ represents the phase rotation at the effective sampling time t_{eff} associated with the (u, v) -th element's delay-time grid position. (21) shows that \mathbf{H}_{eff} jointly captures the large-scale path loss, LEO delay-Doppler coupling, including fractional Doppler, and the FTN-induced ISI via $\mathcal{A}_g(\cdot, \cdot)$. Besides, the term \mathbf{z}^{DD} represents the DD-domain noise vector. Crucially, due to the non-orthogonal FTN pulse shaping and matched filtering, the sampled noise becomes colored. We model TF-domain noise vector $\mathbf{z}_{\text{TF}} \in \mathbb{C}^{MN \times 1}$ as a complex Gaussian process with covariance as

$$\mathbb{E}\{\mathbf{z}_{\text{TF}}\mathbf{z}_{\text{TF}}^H\} = \sigma^2 \mathbf{G}, \quad (22)$$

where \mathbf{G} is a Hermitian Toeplitz correlation matrix determined by the shaping pulses and the FTN compression factor α . The DD-domain noise is then given by $\mathbf{z}^{\text{DD}} = (\mathbf{F}_N \otimes \mathbf{F}_M^H)\mathbf{z}_{\text{TF}}$, where \mathbf{F}_N and \mathbf{F}_M are the normalized DFT matrices.

D. Signal Detection

To recover the transmitted symbol vector \mathbf{x}^{DD} from the received signal in (19), we employ a Linear Minimum Mean-Square Error (LMMSE) detector. While iterative receivers can theoretically approach the performance limits, they are often

ill-suited for power-constrained LEO user terminals (UEs) due to their high computational load and non-deterministic convergence time. In next-generation NTN IoT scenarios, UEs are strictly limited by battery capacity and hardware processing power. The high complexity of iterative schemes translates directly into excessive power drain. Therefore, we deliberately accept a trade-off in BER performance to secure the deterministic low latency and energy efficiency of the LMMSE detector. This ensures that the FTN acceleration gain is not negated by the processing overhead, making the scheme practically deployable in realistic, resource-scarce satellite links. Moreover, it inherently possesses the capability to mitigate the part of structured interference characterizing the LEO-FTN-OTFS system. Specifically, the matrix inversion operation at the core of LMMSE effectively acts as a decorrelator, suppressing the severe ISI induced by aggressive time-domain FTN compression, as well as the residual ICI arising from high-mobility Doppler shifts [21]. Explicitly accounting for the colored noise covariance \mathbf{G} derived in (22), the LMMSE estimate is given by:

$$\hat{\mathbf{x}}^{\text{DD}} = (\mathbf{H}_{\text{eff}}^H \mathbf{H}_{\text{eff}} + \sigma^2 \mathbf{G})^{-1} \mathbf{H}_{\text{eff}}^H \mathbf{y}, \quad (23)$$

where $(\cdot)^H$ denotes the Hermitian transpose, and $\hat{\mathbf{x}}^{\text{DD}} \in \mathbb{C}^{MN \times 1}$ represents the detected symbol vector. The regularization term $\sigma^2 \mathbf{G}$ ensures that the detector minimizes the mean square error without causing excessive noise amplification, which is particularly critical in the non-orthogonal FTN regime.

III. FFTN SIGNALING

Due to the drastic link quality fluctuations in LEO satellite communications, fixed FTN strategies prove suboptimal, as they inevitably suffer from either outages at low elevation angles or spectral inefficiency at high elevation angles. To address this, we propose an LEO-FTN-OTFS scheme that dynamically optimizes α to maximize SE under a strict reliability constraint. The effective SE of an FTN system is given by $\eta(\alpha) = (\log_2 M_{\text{mod}})/\alpha$. Our objective is to maximize $\eta(\alpha)$ by minimizing α , subject to the constraint that the BER remains below a target threshold P_{th} . The instantaneous SNR

Algorithm 1 Flexible FTN-OTFS Transmission Strategy

depends on the transmit power P_{tx} , noise power σ^2 , and the dynamic path loss $L(t)$ at t -th time slot derived in (3), as

$$\gamma(t) = \frac{P_{tx} \cdot 10^{-L(t)/10}}{\sigma^2}. \quad (24)$$

Consequently, the optimization problem regarding the adjustment of α can be formulated as

$$\min_{\alpha \in \mathcal{B}} \quad \alpha \quad \text{s.t.} \quad \text{BER}(\gamma(t), \alpha) \leq P_{\text{th}}, \quad (25)$$

where \mathcal{B} is the set of total K available compression factors, as $\mathcal{B} = \{\alpha_1, \alpha_2, \dots, \alpha_k, \dots, \alpha_K\}$.

However, solving (25) directly is computationally intensive due to the complex ISI-BER relationship. Therefore, we adopt a practical look-up table (LUT) based link adjustment protocol. We define a set of discrete adjustment modes $\{(\alpha_k, \Gamma_k)\}_{k=1}^K$, where Γ_k is the minimum SNR required for mode k . At the transmitter, the specific α for the current frame is selected based on the estimated Channel State Information (CSI) or predicted SNR trajectory:

$$\alpha(t) = \begin{cases} \alpha_K, & \text{if } \gamma(t) \geq \Gamma_K \quad (\text{Aggressive Adjustment}) \\ \alpha_k, & \text{if } \Gamma_k \leq \gamma(t) < \Gamma_{k+1} \\ \dots \\ 1.0, & \text{if } \gamma(t) < \Gamma_1 \quad (\text{Nyquist Back-off}). \end{cases} \quad (26)$$

This design ensures that system opportunistically exploits high SNR during LEO satellite's zenith pass by applying a smaller

α , while reverting to orthogonal transmission at horizon.³

Remarks: It is imperative to highlight that in high-mobility LEO scenarios, the algorithmic optimality often yields to engineering optimality. The LEO channel exhibits extremely short coherence times. Complex iterative optimization algorithms, e.g., exhaustive search or iterative interference cancellation, introduce significant processing latency. By the time such algorithms converge, the channel state may have already drifted, rendering the optimized parameters obsolete. In contrast, our proposed LUT-based strategy offers an $\mathcal{O}(1)$ decision mechanism. This ensures real-time adaptability, allowing the system to track the rapid "horizon-to-zenith" signal evolution without the lag induced by heavy computations. This makes it an "engineering optimal" solution that balances theoretical performance with the strict latency constraints of NTN control loops.

IV. PERFORMANCE ANALYSIS

This section presents a theoretical performance analysis of the proposed LEO-FFTN-OTFS scheme. To evaluate the trade-off between spectral efficiency and reliability, we focus on three critical metrics: Throughput, EE, and BER. These metrics are mathematically derived in Subsections **IV-A**, **IV-B**, and **IV-C**, respectively.

A. Throughput Analysis

1) *Raw Transmission Rate and SE*: Let M_{mod} denote the modulation order. The total information payload in bits per OTFS frame is given by:

$$N_{\text{bits}} = MN \log_2 M_{\text{mod}}. \quad (27)$$

In the proposed LEO-FFTN-OTFS framework, the time-domain FTN signaling imposes a compression factor $\alpha \in (0, 1]$, reducing the fundamental pulse interval to $T_F = \alpha T_0$. Given that an OTFS frame comprises $M \times N$ discretized samples, the effective frame duration is compressed from the Nyquist duration T to:

$$T_{\text{FTN}}(\alpha) \approx MN \times T_F = MN \left(\alpha \frac{T}{MN} \right) = \alpha T. \quad (28)$$

Consequently, the raw data rate R_{raw} is inversely proportional to α , representing the potential acceleration gain:

$$R_{\text{raw}}(\alpha) = \frac{N_{\text{bits}}}{T_{\text{FTN}}(\alpha)} = \frac{MN \log_2 M_{\text{mod}}}{\alpha T}. \quad (29)$$

Furthermore, we define the Raw SE, $\Psi_{\text{raw}}(\alpha)$, to quantify the bandwidth utilization. Assuming a system bandwidth $B \approx 1/T_0$, the SE is derived as:

$$\Psi_{\text{raw}}(\alpha) = \frac{R_{\text{raw}}(\alpha)}{B} \approx \frac{\log_2 M_{\text{mod}}}{\alpha} \quad [\text{bits/s/Hz}], \quad (30)$$

which explicitly demonstrates that $\alpha < 1$ linearly enhances the spectral efficiency beyond the orthogonal limit.

³In this work, we configure three operational modes: Mode 1 (Nyquist) with $\alpha = 1.0$ for low SNR ($\gamma < 0$ dB); Mode 2 (Mild FTN) with $\alpha = 0.95$ for medium SNR ($0 \leq \gamma \leq 15$ dB); and Mode 3 (Aggressive FTN) with $\alpha = 0.9$ for high SNR ($\gamma > 15$ dB).

2) *Effective Throughput*: In practical high-mobility LEO links, the theoretical acceleration is compromised by transmission reliability. We define the effective throughput \mathcal{T}_{eff} as the net rate of successfully decoded bits. Let $P_b(\gamma, \alpha)$ denote the BER, which is a complex function of the instantaneous SNR γ and the interference level determined by α . Assuming that bit errors are independently distributed, the Frame Error Rate (FER), P_{frame} , can be approximated by the probability that at least one bit in the frame is erroneous:

$$P_{\text{frame}}(\gamma, \alpha) = 1 - (1 - P_b(\gamma, \alpha))^{N_{\text{bits}}}. \quad (31)$$

The effective throughput is then the product of the raw rate and the packet success probability:

$$\begin{aligned} \mathcal{T}_{\text{eff}}(\gamma, \alpha) &= R_{\text{raw}}(\alpha) \cdot (1 - P_{\text{frame}}(\gamma, \alpha)) \\ &= \underbrace{\frac{MN \log_2 M_{\text{mod}}}{\alpha T}}_{\text{Acceleration Term}} \cdot \underbrace{(1 - P_b(\gamma, \alpha))^{N_{\text{bits}}}}_{\text{Reliability Penalty}}. \end{aligned} \quad (32)$$

By substituting the elevation-dependent instantaneous SNR $\gamma(\theta_E) = \frac{P_{tx} 10^{-L(\theta_E)/10}}{\sigma^2}$, we establish the analytical relationship between throughput and satellite dynamics:

$$\begin{aligned} \mathcal{T}_{\text{eff}}(\theta_E, \alpha) &= \frac{MN \log_2 M_{\text{mod}}}{\alpha T} \\ &\times \left(1 - P_b\left(\frac{P_{tx} \mathcal{H}(\theta_E)}{\sigma^2}, \alpha\right)\right)^{N_{\text{bits}}}, \end{aligned} \quad (33)$$

where $\mathcal{H}(\theta_E) \triangleq 10^{-L(\theta_E)/10}$ represents the composite channel gain encompassing path loss and atmospheric attenuation.

B. EE

We define the EE metric, η_{EE} , as the number of successfully delivered information bits per Joule of energy consumed. To provide a realistic power consumption model, we consider the inefficiency of the Power Amplifier (PA). The total power consumption P_{total} is:

$$P_{\text{total}} = \frac{P_{tx}}{\xi} + P_c, \quad (34)$$

where $\xi \in (0, 1]$ denotes the drain efficiency of the PA, and P_c represents the fixed circuit power for baseband processing and RF chains. The total energy consumption per frame duration T_{FTN} is thus:

$$E_{\text{frame}}(\alpha) = P_{\text{total}} \times T_{\text{FTN}}(\alpha) = \left(\frac{P_{tx}}{\xi} + P_c\right) \alpha T. \quad (35)$$

Combining (35) with (32), the EE is derived as:

$$\begin{aligned} \eta_{\text{EE}}(\gamma, \alpha) &= \frac{N_{\text{bits}} (1 - P_{\text{frame}}(\gamma, \alpha))}{E_{\text{frame}}(\alpha)} \\ &= \frac{MN \log_2 M_{\text{mod}}}{\left(\frac{P_{tx}}{\xi} + P_c\right) T} \cdot \frac{(1 - P_b(\gamma, \alpha))^{N_{\text{bits}}}}{\alpha}. \end{aligned} \quad (36)$$

Equation (36) reveals a dual benefit of aggressive FTN ($\alpha < 1$) in the high-SNR regime: it boosts data rate while simultaneously reducing the energy consumption window, thereby linearly improving η_{EE} .

C. Theoretical BER

To quantify $P_b(\gamma, \alpha)$, we derive the theoretical performance of the LMMSE detector. Consider the vectorized DD-domain input-output relation $\mathbf{y} = \mathbf{H}_{\text{eff}} \mathbf{x}^{\text{DD}} + \mathbf{z}^{\text{DD}}$. The noise vector \mathbf{z}^{DD} follows a zero-mean multivariate complex Gaussian distribution $\mathcal{CN}(\mathbf{0}, \mathbf{R}_z)$, where the covariance matrix captures the colored noise characteristics induced by non-orthogonal FTN filtering:

$$\mathbf{R}_z = \sigma^2 \underbrace{(\mathbf{F}_N \otimes \mathbf{F}_M^H) \mathbf{G} (\mathbf{F}_N \otimes \mathbf{F}_M^H)^H}_{\triangleq \tilde{\mathbf{G}}}, \quad (37)$$

where $\mathbf{F}_N \in \mathbb{C}^{N \times N}$ and $\mathbf{F}_M \in \mathbb{C}^{M \times M}$ denote the normalized Discrete Fourier Transform (DFT) matrices of dimensions $N \times N$ and $M \times M$, respectively. The LMMSE detector seeks a linear filter matrix $\mathbf{W} \in \mathbb{C}^{MN \times MN}$ that produces an estimate $\hat{\mathbf{x}}^{\text{DD}} = \mathbf{W} \mathbf{y}$ minimizing the aggregate Mean Square Error (MSE):

$$\mathbf{W}_{\text{opt}} = \arg \min_{\mathbf{W}} \mathbb{E} [\|\mathbf{x}^{\text{DD}} - \mathbf{W} \mathbf{y}\|^2]. \quad (38)$$

Solving (38) via the orthogonality principle (Wiener-Hopf equation) $\mathbb{E}[(\mathbf{x}^{\text{DD}} - \hat{\mathbf{x}}^{\text{DD}}) \mathbf{y}^H] = \mathbf{0}$, and assuming normalized signal power $\mathbb{E}[\mathbf{x}^{\text{DD}} (\mathbf{x}^{\text{DD}})^H] = \mathbf{I}_{MN}$, we obtain:

$$\begin{aligned} \mathbf{W}_{\text{opt}} &= \mathbf{H}_{\text{eff}}^H (\mathbf{H}_{\text{eff}} \mathbf{H}_{\text{eff}}^H + \mathbf{R}_z)^{-1} \\ &\stackrel{(a)}{=} (\mathbf{H}_{\text{eff}}^H \mathbf{R}_z^{-1} \mathbf{H}_{\text{eff}} + \mathbf{I}_{MN})^{-1} \mathbf{H}_{\text{eff}}^H \mathbf{R}_z^{-1}, \end{aligned} \quad (39)$$

where (a) follows from the matrix inversion lemma. Substituting $\mathbf{R}_z = \sigma^2 \tilde{\mathbf{G}}$, the LMMSE weight matrix is rigorously expressed as

$$\mathbf{W} = \left(\mathbf{H}_{\text{eff}}^H \tilde{\mathbf{G}}^{-1} \mathbf{H}_{\text{eff}} + \sigma^2 \mathbf{I}_{MN}\right)^{-1} \mathbf{H}_{\text{eff}}^H \tilde{\mathbf{G}}^{-1}. \quad (40)$$

The post-detection error covariance matrix $\Phi \triangleq \mathbb{E}[(\mathbf{x}^{\text{DD}} - \hat{\mathbf{x}}^{\text{DD}}) (\mathbf{x}^{\text{DD}} - \hat{\mathbf{x}}^{\text{DD}})^H]$ is given by:

$$\begin{aligned} \Phi &= (\mathbf{I}_{MN} + \mathbf{H}_{\text{eff}}^H \mathbf{R}_z^{-1} \mathbf{H}_{\text{eff}})^{-1} \\ &= \sigma^2 \left(\sigma^2 \mathbf{I}_{MN} + \mathbf{H}_{\text{eff}}^H \tilde{\mathbf{G}}^{-1} \mathbf{H}_{\text{eff}}\right)^{-1}. \end{aligned} \quad (41)$$

The effective Signal-to-Interference-plus-Noise Ratio (SINR) for the i -th symbol, $\gamma_{\text{eff},i}$, is inversely related to the diagonal elements of the error covariance matrix. Let $\text{MSE}_i = [\Phi]_{i,i}$ denote the i -th diagonal element. Based on the unbiased estimator assumption [22], the effective SINR is:

$$\gamma_{\text{eff},i} = \frac{1}{\text{MSE}_i} - 1 = \frac{1}{[\Phi]_{i,i}} - 1. \quad (42)$$

Consequently, according to [23], [24], the average BER for an M_{mod} -ary QAM constellation is approximated by averaging the conditional error probabilities over all DD bins:

$$P_b(\gamma, \alpha) \approx \frac{c_1}{MN} \sum_{i=1}^{MN} Q(\sqrt{c_2 \cdot \gamma_{\text{eff},i}}), \quad (43)$$

where the modulation-specific constants are $c_1 = \frac{4}{\log_2 M_{\text{mod}}} (1 - \frac{1}{\sqrt{M_{\text{mod}}}})$ and $c_2 = \frac{3}{M_{\text{mod}} - 1}$.

TABLE II
SIMULATION PARAMETERS

Parameter	Value
Carrier Frequency (f_c)	28 GHz (Ka-band)
Satellite Altitude (h_{sat})	780 km
System Bandwidth	10 MHz
Subcarrier Spacing (Δf)	15 kHz
Modulation Order (M_{mod})	2 (BPSK) or 4 (QPSK)
Pulse Shaping Filter	RRC
Roll-off Factor (β)	0.3
Filter Span (L_{span})	6 symbols
Zenith Atmos. Attenuation (A_{zenith})	0.22 dB
Channel Models	3GPP TR 38.811

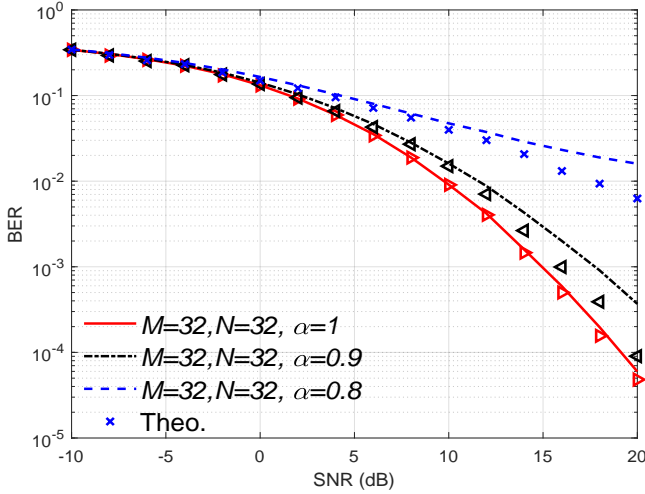


Fig. 3. Theoretical and simulation BER performance of LEO-FTN-OTFS scheme with $M = N = 32$, TDL-A, and different α .

V. NUMERICAL RESULTS

In this section, we present a comprehensive numerical evaluation of the proposed LEO-FFTN-OTFS scheme employing the LMMSE detector. To reflect a realistic orbital scenario, we consider a LEO satellite configuration operating at an altitude of $h_{\text{sat}} = 780$ km in the Ka-band, with a carrier frequency of $f_c = 28$ GHz. The system bandwidth is allocated as $B = 10$ MHz with a subcarrier spacing of $\Delta f = 15$ kHz, yielding a symbol duration of $T = 1/\Delta f \approx 66.7$ μ s. Regarding the FTN signaling parameters, a RRC pulse with a roll-off factor $\beta = 0.3$ is adopted, and the filter truncation length is set to $L_{\text{span}} = 6$ symbols to balance complexity and performance. For the modulation constellation, we evaluate both $M_{\text{mod}} = 2$ (BPSK) and 4 (QPSK). To capture the diverse propagation characteristics of LEO environments, the channel models are rigorously aligned with the standard 3GPP TR 38.811 technical specifications [15], [16], incorporating various TDL profiles ranging from NLoS to LoS dominant scenarios. Monte Carlo simulations are performed with 6×10^3 iterations per SNR point. The key simulation parameters are summarized in Table II.

The validity of the derived theoretical BER bounds against simulation results is examined in Fig. 3. First, according to results, we can find that the LEO-OTFS-FTN scheme can achieve satisfactory BER performance. Moreover, it is

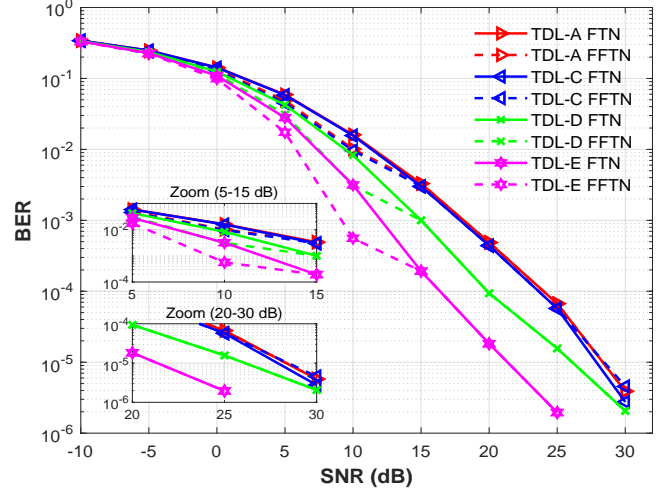


Fig. 4. BER performance of various TDL models with FTN and FFTN applied in LEO-OTFS system with $M = N = 16$ and $\alpha = 0.9$.

observed that for the orthogonal Nyquist signaling case, i.e., $\alpha = 1$, the simulation results exhibit similar performance to the theoretical predictions especially within the low SNR range, confirming the accuracy of the derived analytical framework. However, as the time-domain compression factor α decreases, a noticeable discrepancy emerges between the theoretical bounds and simulated performance, particularly in the high SNR regime, e.g., $\text{SNR} > 15$ dB. Specifically, with more aggressive compression, i.e., smaller α , the simulation curves deviate from the theoretical bounds and manifest a distinct error floor. This phenomenon is attributed to the residual ISI and the severe coloring of the noise spectrum induced by FTN, which limit the efficacy of the linear LMMSE detector at high SNRs. This limitation underscores the necessity of the proposed adaptive FFTN strategy, which avoids aggressive compression modes in scenarios where residual interference would dominate.

Fig. 4 delineates the BER performance across different channel profiles. The TDL-E model achieves the superior performance, followed by TDL-D, whereas the TDL-A model exhibits the worst degradation. This performance hierarchy stems from the varying degrees of LoS components. TDL-E and TDL-D represent open/rural environments characterized by strong Ricean K -factors, which significantly mitigate the deep fading effects prevalent in the NLoS, Rayleigh-fading dominated TDL-A environment. Crucially, the proposed FFTN scheme demonstrates superior reliability compared to fixed aggressive FTN schemes, particularly in the low SNR regime. In the high SNR region, the BER of the FFTN scheme seamlessly converges to that of the fixed FTN with $\alpha = 0.9$, indicating that the adaptive strategy successfully exploits the aggressive compression mode to maximize spectral efficiency when channel quality permits.

Fig. 5 presents the effective throughput of the proposed FFTN scheme compared to fixed FTN benchmarks with $\alpha \in \{1.0, 0.9, 0.8\}$. The results in Fig. 5 (a) explicitly illustrate the limitations of static configurations. The aggressive $\alpha = 0.8$ mode suffers from a catastrophic throughput collapse in the

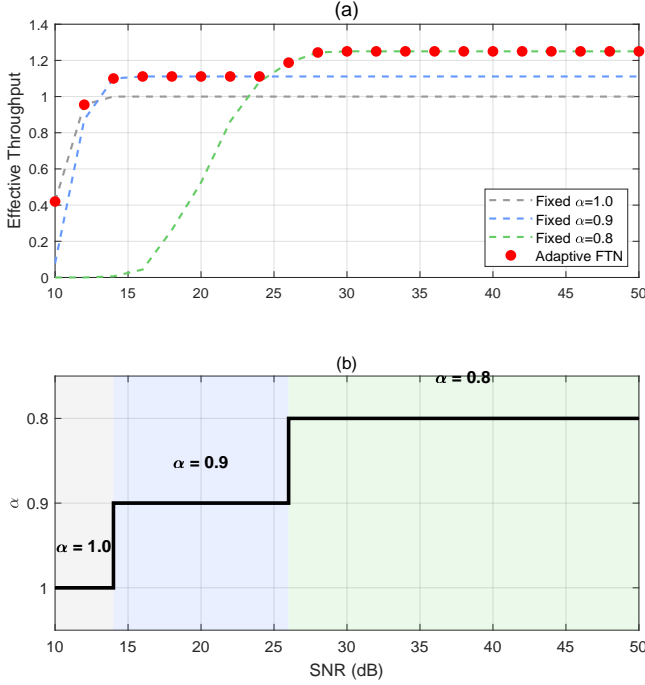


Fig. 5. Effective throughput and α trend of LEO-FFT-OTFS, LEO-OTFS with $\alpha = 1$, and LEO-FTN-OTFS with $\alpha = 0.9$ and 0.8 , as well as $M = 32$, $N = 16$, and $M_{\text{mod}} = 4$.

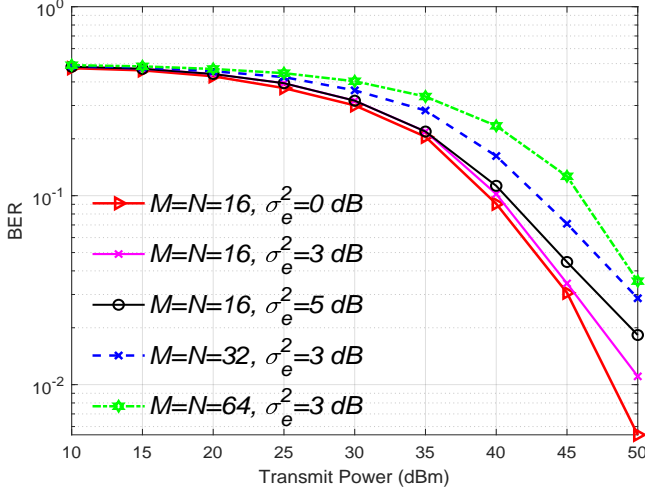


Fig. 6. BER performance of the proposed scheme with a realistic SNR estimation uncertainty modeled by a generalized Gaussian error term in TDL-B model.

low-SNR regime (< 15 dB) due to excessive ISI-induced frame errors, rendering the link unusable. Conversely, the conservative $\alpha = 1.0$ mode ensures connectivity but hits a throughput saturation ceiling early, failing to convert the excess SNR budget into higher data rates. In contrast, the results clearly show that the FFTN acts as an upper envelope to the fixed schemes, consistently achieving the highest possible throughput across entire SNR range. System transitions from $\alpha = 1.0$ to $\alpha = 0.9$ at around 14 dB, and further to $\alpha = 0.8$ around 26 dB, ensuring an optimal trade-off between reliability and throughput. The underlying mechanism is detailed in Fig. 5 (b), which depicts the discrete α transitions derived

from the LUT. We observe three distinct operational zones: 1) The system defaults to the Nyquist mode ($\alpha = 1.0$) to maintain basic link connectivity against noise in $\text{SNR} < 14$ dB. 2) As channel conditions improve, the system switches to $\alpha = 0.9$, balancing acceleration with interference management, within $\text{SNR} = 14\text{--}26$ dB. 3) In the high-SNR regime, the system confidently adopts the aggressive $\alpha = 0.8$ mode. Notably, this yields a significant 25% throughput gain, scaling by factor $1/\alpha \approx 1.25$, compared to the conventional Nyquist baseline when $\text{SNR} > 26$ dB. This step-wise adaptation ensures that the system always operates at the optimal point where reliability constraints are met while maximizing SE.

Given the highly dynamic nature of LEO links, obtaining perfect knowledge of the link quality is practically challenging. The impact of imperfect CSI estimation, i.e., errors in channel impulse response coefficients, on signal detection is beyond the scope of this study and assumes perfect CSI for the LMMSE detector. To model the uncertainty in link quality assessment, we introduce a Gaussian error term $\Delta_{\text{dB}} \sim \mathcal{N}(0, \sigma_e^2)$ to the estimated SNR. Fig. 6 evaluates the robustness of the proposed scheme under this uncertainty. With a fixed grid size of $M = N = 16$, the BER performance degrades only marginally as the standard deviation of the SNR estimation error σ_e , increases from 0 dB to 5 dB. This indicates that the designed FFTN strategy possesses strong resilience to moderate SNR estimation imperfections, as the LUT includes sufficient margins to accommodate fluctuations. However, when the estimation error is significant, e.g., fixed at 3 dB, increasing the OTFS grid dimensions from 16 to 64 results in a noticeable performance penalty. This suggests that larger frame sizes, while offering higher Doppler resolution, are more sensitive to mode mismatch caused by inaccurate SNR estimation, necessitating a trade-off between frame size and robustness.

VI. CONCLUSION

In this paper, we investigated a lightweight LEO-FFT-OTFS transmission scheme tailored for power-constrained satellite platforms. For our design, we conducted a comprehensive theoretical analysis, deriving analytical expressions for the BER, throughput, and EE to benchmark the system performance. We evaluated the performance under realistic 3GPP TR 38.811 channel models and observed that LOS scenarios exhibited superior BER performance compared to NLOS scenarios. Crucially, simulation results confirmed that the proposed low-complexity adaptive strategy effectively resolved the error floor issue of fixed FTN systems by dynamically adjusting the compression factor. By minimizing computational overhead, this approach proved effective in mitigating channel aging effects caused by processing latency in high-mobility scenarios. Thus, the LEO-FFT-OTFS scheme achieved an optimal trade-off between reliability, computational efficiency, and SE, maximizing the effective throughput across the entire SNR range. Ultimately, this study addressed the specific constraints of Doppler shifts, limited bandwidth, and onboard energy scarcity, contributing vital insights for future green LEO satellite communications.

REFERENCES

- [1] Z. Xiang *et al.*, "Massive MIMO uplink transmission for multiple LEO satellite communication," *IEEE Trans. Aerosp. Electron. Syst.*, vol. 61, no. 2, pp. 4852–4865, Apr. 2025.
- [2] C. Zhang, *et al.*, "Unlocking potential in LEO satellite communications through spatial modulation and space shift keying," *IEEE Open J. Commun. Soc.*, vol. 6, pp. 9862–9878, 2025.
- [3] X. Zhang *et al.*, "Relay-satellite-assisted LEO constellation NOMA communication system," *IEEE Trans. Aerosp. Electron. Syst.*, vol. 61, no. 1, pp. 995–1011, Feb. 2025.
- [4] Y. Li, P. Yue, Z. Song, S. Wang, G. Pan, and J. S. Thompson, "A signal reacquisition based on cross-entropy and postdetection with data modulation for LEO satellite communications," *IEEE Trans. Aerosp. Electron. Syst.*, vol. 61, no. 6, pp. 18067–18080, Dec. 2025.
- [5] Z. Zhang, M. Yuksel, G. M. Guvensen, and H. Yanikomeroglu, "Capacity and IAPR analysis for MIMO faster-than-Nyquist signaling with high acceleration rate," *IEEE Trans. Wireless Commun.*, vol. 25, pp. 1451–1466, 2026.
- [6] Q. Deng, Y. Ge, and Z. Ding, "A unifying view of OTFS and its many variants," *IEEE Commun. Surveys Tuts.*, vol. 27, no. 6, pp. 3561–3586, Dec. 2025.
- [7] U. Mengali, "Synchronization of QAM signals in the presence of ISI," *IEEE Trans. Aerosp. Electron. Syst.*, vol. AES-12, no. 5, pp. 556–560, Sep. 1976.
- [8] H. Xu, *et al.*, "FTN-assisted SWIPT-NOMA design for IoT wireless networks: A paradigm in wireless efficiency and energy utilization," *IEEE Sensors J.*, vol. 25, no. 4, pp. 7431–7444, Feb. 2025.
- [9] O. Tokluoglu, A. Cicek, E. Cavus, E. Bedeer, and H. Yanikomeroglu, "GRU-based sequence detection for faster-than-Nyquist signaling," *IEEE Open J. Veh. Technol.*, 2025.
- [10] C. Zhang, *et al.*, "What roles can spatial modulation and space shift keying play in LEO satellite-assisted communication?," in *Proc. IEEE Virt. Conf. Commun. (VCC)*, 2024, pp. 1–6.
- [11] X. Zhao, Z. Liu, B. Lyu, Y. Du, and G. Zhang, "Block time-varying channel estimation for OTFS systems in LEO satellite communications," *IEEE Trans. Aerosp. Electron. Syst.*, vol. 62, pp. 1119–1131, 2026.
- [12] Y. He, X. Wang, and Z. Dou, "Collaborative method for OTFS channel estimation and prediction based on LEO satellite-ground link," *IEEE Trans. Cogn. Commun. Netw.*, vol. 12, pp. 3452–3467, 2026.
- [13] H. Xu, *et al.*, "Adaptive damping log-domain message-passing algorithm for FTN-OTFS in V2X communications," *Sensors*, vol. 25, no. 12, p. 3692, Jun. 2025.
- [14] X. Wang, S. Gong, W. Shen, C. Xing, and J. A. Zhang, "Multi-carrier faster-than-Nyquist signaling for OTFS systems," *IEEE Trans. Veh. Technol.*, vol. 74, no. 12, pp. 19339–19354, Dec. 2025.
- [15] *Propagation data and prediction methods required for the design of Earth-space telecommunication systems*, ITU-R Recommendation P.618-14, Aug. 2023.
- [16] *Attenuation by atmospheric gases*, ITU-R Recommendation P.676-13, Aug. 2022.
- [17] C. Zhang, I. Cheng Wong, B. K. Ng, and C.-T. Lam, "LEO satellite-assisted GSSK with optimized antenna combination selections and detector," *IEEE Commun. Lett.*, vol. 29, no. 6, pp. 1210–1214, Jun. 2025.
- [18] "LTE, technical specification group radio access network; study on new radio (NR) to support non-terrestrial networks (release 15), v15.3.0," 3GPP, Sophia Antipolis, France, Rep. TR 38.811, Jul. 2020.
- [19] *LTE, Evolved Universal Terrestrial Radio Access (E-UTRA); Base Station (BS) Radio Transmission and Reception, Version 8.6.0, Release 8*, 3GPP Standard TS 36.104, Jul. 2009.
- [20] A. S. Bora, K. T. Phan, and Y. Hong, "IRS-assisted high mobility communications using OTFS modulation," *IEEE Wireless Commun. Lett.*, vol. 12, no. 2, pp. 376–380, Feb. 2023.
- [21] J. G. Proakis and M. Salehi, *Digital Communications*, 5th ed. New York, NY: McGraw-Hill, 2008.
- [22] M. Tüchler, R. Koetter, and A. C. Singer, "Turbo equalization: Principles and new results," *IEEE Trans. Commun.*, vol. 50, no. 5, pp. 754–767, May 2002.
- [23] A. Goldsmith, *Wireless Communications*. Cambridge, UK: Cambridge University Press, 2005.
- [24] T. Domínguez-Bolaño, J. Rodríguez-Piñeiro, J. A. García-Naya, and L. Castedo, "Bit error probability and capacity bound of OFDM systems in deterministic doubly-selective channels," *IEEE Trans. Veh. Technol.*, vol. 69, no. 10, pp. 11458–11469, Oct. 2020.